https://doi.org/10.5194/egusphere-2026-2347
Preprint. Discussion started: 21 May 2026

Assessing sedimentological proxies for characterizing tropical storm deposits in the Chandipur coastal region of Bay of Bengal, India: A modern analog for paleotempestology

KOUSHIK SAHA[1], ANTAREEP NANDY[1], KALBEN WANCHU BHUTIA[1], JOHN S. ARMSTRONG-ALTRIN[2]

Correspondence to: Dr. Koushik Saha (ORCiD: https://orcid.org/0000-0003-2412-2478)
Email: koushiksaha09@gmail.com

[1]Department of Geology, University of North Bengal, Siliguri, West Bengal, India.
[2]Unidad de Procesos Oceánicos y Costeros, Instituto de Ciencias del Mar y Limnología, Universidad Nacional Autónoma de México, Ciudad Universitaria, Ciudad de México 04510, CDMX, México.

https://doi.org/10.5194/egusphere-2026-2347
Preprint. Discussion started: 21 May 2026

Abstract

Coastal morphodynamics in barrier systems are governed by changes in sediment supply, sea level, and storm events. However, the limited availability of well-characterized modern analogs hinders the interpretation of sediments deposited by tropical storms, particularly in the Bay of Bengal. This study aims to evaluate the sedimentological proxies for identifying overwash deposits in the back-barrier region of Chandipur, India, using integrated granulometric and morphoscopic analyses across five sediment transects. Grain size distributions were modeled into four end-members (EMs) representing aqueous suspension-dominated transport, aqueous suspension with minor saltation, aeolian saltation, and high-energy depositional environment. To address compositional constraints, centered log-ratio (Clr)-transformed EM scores, were analyzed spatially to assess variations in depositional processes. Quartz grain morphoscopy, following the Cailleux classification, was used to assign grains to seven established shape categories, with fractured C-type grains being interpreted as indicative of high-energy mechanical modification. By combining grain size and morphoscopic characteristics, cluster analysis distinguished three sediment groups linked to aqueous, aeolian, and overwash-dominated environments. Microtextural observations further refine transport interpretations, indicating that many grains underwent high-energy collisions typical of marine reworking during storm events. A multi-proxy approach incorporating EM modelling, compositional analysis, grain morphology, and microtextural evidence establishes a reliable framework for differentiating overwash deposits. The results emphasize the value of integrating multiple sedimentological proxies to identify tropical storm signatures, with clear applications in paleotempestology and coastal management initiatives.

Keywords: Coastal barrier environment; Tropical storm; Granulometry; Cailleux analysis; microtexture

https://doi.org/10.5194/egusphere-2026-2347
Preprint. Discussion started: 21 May 2026

1. Introduction

The future of global coastlines depends on their capacity to adapt to accelerated sea-level rise (SLR) and increasing storm intensity (Cooper et al., 2018; FitzGerald et al., 2018). Due to their position at the land–sea interface, coastal barrier systems are particularly vulnerable to climate change, driven by the combined influence of atmospheric and oceanic stressors like SLR, cyclones, and storms (Arkema et al., 2013; Zinnert et al., 2017; Zinnert et al., 2019). During cyclonic storms, storm surges sediments landward through overwash processes, leading to significant redistribution of sediments across coastal barriers and associated morphological changes that may eventually surpass pre-storm configurations (Bullard et al., 2019). SLR further enhances the inland penetration of storms and waves, promoting landward movement of barrier systems (Masselink and van Heteren, 2014). Consequently, these processes influence the rapid evolution of coastal barriers and adjacent wetland ecosystems, highlighting the importance of understanding their behaviour in response to catastrophic storms and cyclones.

Paleotempestology, a recognized approach for revealing past storm patterns, provides long-term information for storm variability projections. During storm landfall, storm surges may breach beach barriers, transporting beach and marine sediments to create a storm-surge or overwash deposits in back-barrier areas. Numerous researchers have used geochemical proxies to comprehend the paleotempestology of the tropical coastal deposits (Bianchette et al., 2022; Williams et al., 2022; Yao et al., 2021; Stewart et al., 2017); however, the controversy surrounding the effectiveness of a few geochemical proxies in identifying storm-surge deposits persists (Yao et al., 2023). Moreover, the overwash deposits are likely contain marine microfossils, because the storm surges produce sediment excavation and landward transportation and deposition of microfossils. Although the presence of the fossils might not be available in all of the deposited layers (Yao et al., 2023; Hawkes and Horton, 2012) the granulometric analysis of storm-induced overwash deposits, aids in the comprehension of

https://doi.org/10.5194/egusphere-2026-2347
Preprint. Discussion started: 21 May 2026

sediment transport mechanisms and the assessment of sedimentary characteristics, provenance, and depositional processes of storm deposits (Hong et al., 2018; Bennington and Farmer, 2015; Williams, 2015; Castagno et al., 2021; Ketthong et al., 2024 a,b). The characterization of sediment grain size, which is influenced by a range of transport processes, is commonly achieved through the application of end-member mixing analysis (EMMA) to accurately describe the specific processes (Paterson and Heslop, 2015; Van Hateren et al., 2018; Yang et al., 2022). The granulometric textures of washover sand deposits at Tiana Beach, Long Island, New York, were utilized to distinguish overwash episodes produced by Superstorm Sandy (Bennington and Farmer, 2015). Moreover, sand encroachment patterns in oases ecosystems have been successfully established with granulometric analysis, EMMA modelling and multivariate compositional data processing (Puy et al., 2018). The morphology of quartz sands, on the other hand, offers significant insights into the processes that govern sediment deposition. Quartz grain morphoscopy significantly helps in distinguishing storm deposits in the coastal deposits of the Baltic region (Kalińska-Nartiša et al., 2018, 2024). Even the sedimentary environment along the Brazilian coast has been reconstructed by combining granulometric investigations with the optical appearance of quartz grains (Machado et al., 2016). Recently, the sedimentary transport process and depositional environment along the Bay of Bengal coastal region of Bangladesh have been studied with microtextural evidence on the quartz grains (Hossian et al., 2024). Moreover, the transportation and deposition of quartz grains resulting from tsunamis and storm waves exhibit distinct microtextural characteristics attributed to the intense marine inundations associated with high-energy mechanical modification (Costa et al., 2012, 2017,2021; Kalińska-Nartiša et al., 2018, 2022; Yhasnara et al., 2023).

To investigate modern analogs of tropical paleotempestological deposits, we selected the coastal barrier-estuary system of Chandipur on the northeastern coast of the Bay

https://doi.org/10.5194/egusphere-2026-2347
Preprint. Discussion started: 21 May 2026

of Bengal, India. This region is regarded as one of the most vulnerable regions to SLR and intensifying tropical storms (Hoque et al., 2025). Over the past 45 years, sea surface temperature (SST) in the Bay of Bengal has increased by ~ 0.2–0.3°C, with projected warming of 2.0–3.5°C by the end of the current century (Rajalakshmi and Achyuthan, 2021), contributing to accelerated SLR and an increase in the intensity of cyclones (Bushra et al., 2019; Sahoo and Bhaskaran, 2018). The resulting storm surge risk is amplified by the semi-enclosed form of the ocean, bathymetry of the continental shelf, and tidal amplitudes (Chan and Kepert, 2010), as well as the presence of a barrier-estuary system and the shallow nature of the shelf. Although integrated approaches combining granulometry, micromorphology, end-member modelling, and multivariate statistics are effective for identifying storm deposits (Leszczyńska et al., 2024), their application in the Bay of Bengal remains limited. Given the preservation biases and site-specific nature of proxy records in paleotempestology, calibration with modern event deposits is essential. Accordingly, this study employs a combination of different sedimentological techniques, i.e., granulometric and grain surface morphological analysis, along with microtextural analysis to characterize storm-derived sediments. The objective is to understand sediment provenance, depositional processes, and energy conditions associated with tropical events, thereby providing a modern analog framework for paleotempestological reconstructions and supporting improved coastal hazard assessment

2. Study area

The coastal barrier–estuary system of Chandipur, Balasore, on the northeastern coast of India, was chosen as the study site (Figure 1). The occurrence of disastrous storm surges in the Bay of Bengal, in comparison to other regions worldwide, can be attributed to several factors. These factors include the convergence of the bay with a funnel-shaped configuration, the presence of a wide continental shelf that encompasses the deltaic environment in the Bay of Bengal, a low-

https://doi.org/10.5194/egusphere-2026-2347
Preprint. Discussion started: 21 May 2026

97 lying coastal belt, high tidal range, the presence of numerous riverine systems, tidal creeks,
98 mudflats, and a complex geomorphic environment. These combined factors contribute to the
99 heightened vulnerability of the Bay of Bengal to storm surges (Bushra et al., 2019). The study
100 area is situated near the mouth of the Buribulum River along an arcuate coastal stretch of the
101 Bay of Bengal. This barrier-estuarine coast of Balasore is characterized by an intertidal flat, a
102 shore-parallel sandy barrier trending NE-SW, and a marshland dominated back-barrier
103 environment (Chakrabarti, 2005; Saha et al., 2022). The back-barrier marsh ecosystem is
104 endowed with several kinds of vegetation species like *Porteresia coarctata* (C_3), *Leersia*
105 *hexandra* (C_3),*Suaeda nudiflora* (C_3), *Suaeda maritime* (C_3), *Myriostachya wightiana* (C_4),
106 *Paspalum vaginatum* (C_4), *Sesuvium portulacastrum* (C_4), *Acanthus ilicifolius*(C_3) (Saha et al.,
107 2022). The barrier–estuary system is influenced by a mesotidal regime with a semi-diurnal tidal
108 character (Chakrabarti, 2005; Mukherjee et al., 1987; Saha & Sinha, 2023). Hydrodynamic
109 conditions are governed by waves predominantly approaching from the south and southeast
110 (Saha et al., 2023), generating a northward-directed littoral drift system. Additionally,
111 prevailing winds predominantly originate from the southeast during most of the seasons and
112 impact the coastal processes and sediment reworking within the barrier–estuary system.

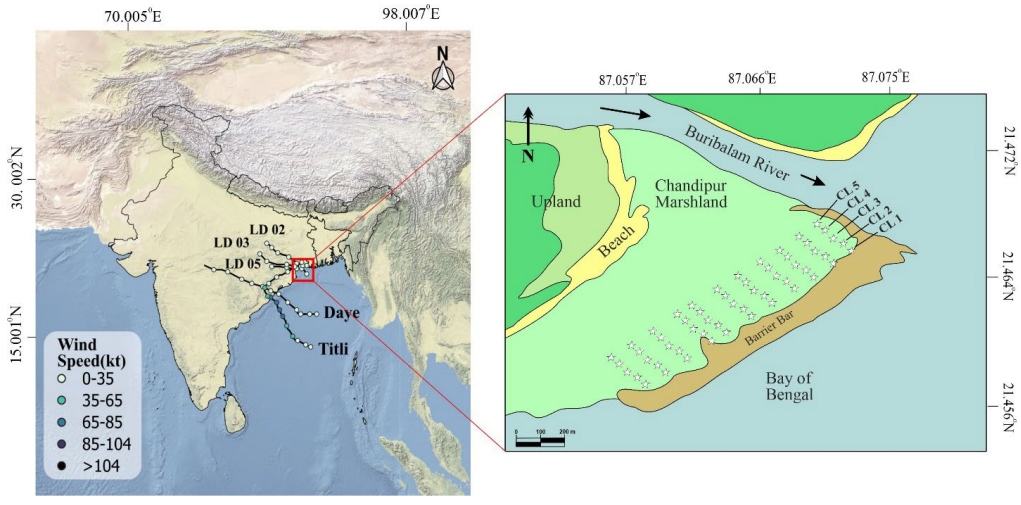

113

https://doi.org/10.5194/egusphere-2026-2347
Preprint. Discussion started: 21 May 2026

Figure 1: The map displays the storm events in Bay of Bengal region around Chandipur, along with the sampling locations for the five transects.

3. Materials and methods

In 2018, surface sediments were collected from five shore-parallel transects (NE–SW orientation) spaced 50 m apart. Sampling was conducted at 150 m intervals along each transect, with 11 samples obtained from each (Figure 1). Sediment samples were collected from the top ~10 cm of surface, which were then carefully stored in plastic bags. Subsequently, the samples were dried in a hot-air oven maintained at a temperature of 50º C.

3.1 Grain size analysis and end-member modelling

The laser diffraction method was employed for the purpose of measuring grain size. 0.5 grams of desiccated sediments were subjected to a pretreatment process involving the addition of 10 milliliters of 20 % hydrogen peroxide (H_2O_2) and 10 milliliters of 10% hydrochloric acid (HCl). This pretreatment was aimed to eliminate organic matter and carbonates from the sediments. Subsequently, a volume of 100 ml of distilled water was introduced to the samples, which were then allowed to settle for a duration of 12 hours. Following that, a volume of 10 mL of a 0.05 normal solution of sodium hexametaphosphate $(NaPO_3)_6$ was introduced into the sample before conducting the measurement. The measurements of all samples were conducted using the Partica mini-LA-350, a laser granulometer manufactured by Horiba Scientific at the laboratory of the University of North Bengal, India. As suggested by Paterson and Heslop (2015), the grain-size distributions were analyzed using the Weibull function, to separate the process-related components. End-member modeling analysis (EMMA) is a flexible and robust statistical method used to unmix complex sediment grain-size distributions (GSDs) into their fundamental, constituent components, known as end-members. The core of the method is a linear mixing model expressed in matrix notation as Y = SC + E. In this equation, Y is the data

https://doi.org/10.5194/egusphere-2026-2347
Preprint. Discussion started: 21 May 2026

matrix of observed GSDs, S is the matrix of end-member GSDs, C is the matrix of end-member proportions for each sample, and E is the error matrix. The AnalySize software, which was developed in MATLAB, employs a complex unmixing technique known as Hierarchical Alternating Least Squares Non-Negative Matrix Factorization (HALS-NMF) to resolve this equation. The procedure commences with an initialization phase. The Splitting Augmented Lagrangian (SISAL) algorithm is employed to approximate the end-member distributions, while the fully constrained least squares technique is employed to approximate the end-member abundances. The end-member and abundance matrices are incrementally enhanced by following this configuration. This process is repeated until it converges to an optimal solution, ensuring that both end-members and their proportions are subject to non-negative and unit-sum constraints, reflecting their physical reality. The quality of the final model is assessed using metrics like the coefficient of determination (R^2) and the angular difference between the observed data and the model's results, which helps to determine the appropriate number of end-members for the analysis. The outcomes of the end-member analysis (EMMA) were acquired through the execution of AnalySize v1.1.1 in MATLAB, as described by Paterson and Heslop (2015).

3.2 Grain morphoscopic and microtextural study

In addition to the granulometric analysis, grain exoscopic analyses were performed on all the samples of the five transects. About 200 grams of the sample was sieved for 20 minutes using different sieve sizes: 1.0, 0.8, 0.5, 0.315, 0.25, 0.2, 0.125, 0.1, and 0.063 mm, following the method of Mycielska-Dowgiałło (2007). The roundness and surface features of grains were determined by a Nikon microscope with a magnification of 50x following Kalinska-Nartisa et al. (2018). The characteristics of quartz grains were classified according to two criteria: (1) grain shape, which includes angular, partially rounded, and well-rounded shapes, and (2) surface type, which includes matte and shiny surfaces following the Cailleux (1942)

https://doi.org/10.5194/egusphere-2026-2347
Preprint. Discussion started: 21 May 2026

methodology, subsequently extended by Mycielska-Dowgiałło and Woronko (1998). Based on this classification, quartz grains are grouped into seven distinct categories, each of which corresponds to specific sedimentary environments. These categories are as follows: (1) RM, characterized by a well-rounded shape and a matte surface that covers the entire grain surface, (2) EM/RM, which exhibits a partially-rounded shape and a matte surface limited to the most convex parts of the grain, (3) EL, well-rounded shape and a shiny surface, formed in a high-energy aqueous environment, (4) EM/EL, partially rounded grains with shiny surfaces, indicative of an aqueous environment, (5) NU, angular fresh grains that show no visible transportation trails and have sharp grain edges due to minimal chemical weathering, (6) C, broken grains, with some portion of the original grain cracked, and (7) O, Lastly, grains with intense precipitation of silica. For scanning electron microscopy (SEM), approximately twenty grains (fine to coarse-grained) from each sample, were selected and processed based on the chemical pretreatment procedures of Vos et al. (2014) and Saha and Sinha (2023). Subsequently, the grains were affixed to an aluminum stub using double-sided carbon tape and subjected to a gold coating. Ultimately, a selection was made from the grains, which were subsequently subjected to photographic documentation using a JSM IT100 instrument to identify surface microtexture following the procedure of Mahaney (2002) and Vos et al. (2014). To comprehend and delineate the effects of the storm, characteristic of a specific microtextural family is presented semi-quantitatively through the analysis of their respective proportions of grain surface occupation (Costa et al., 2012; Bellanova et al., 2016; Kalinska-Nartisa et al., 2024). The angularity of the grains was classified using the Powers scale (Powers, 1953). For understanding the temsological modulation of the grains, four groups of microtextural features are considered: (1) fresh surfaces, (2) percussion marks, (3) adhering particles, and (4) dissolution (Costa et al. 2012, Kalinska-Nartisa et al., 2024).

https://doi.org/10.5194/egusphere-2026-2347
Preprint. Discussion started: 21 May 2026

3.3 Statistical analysis

The relevance of compositional log-transformations in geochemical and granulometric data has been demonstrated in recent sediment geochemical research (Buccianti et al., 2015; Flood et al., 2016; Saha et al., 2024). The ideal compositional dataset is one that sums to 1 or 100%, and granulometric datasets are prominent examples of this (van den Boogaart & Tolosana-Delgado, 2008). Each granulometric dataset is divided by the geometric mean of size classes analyzed and subsequently log-transformed using the centered log-ratio (clr) transformation for closure effect and nonnormality (Aitchison, 1986).

Clr-transformed variables have been successfully employed to map elemental concentrations and to visualize the relative contribution of each granulometric EM in a regional dataset (Reimann et al., 2012; Puy et al., 2018). We also used clr log transformation on the end-member (EM) scores to enhance the visualization of the relative contribution of each EM within the dataset. Principal component analysis (PCA) is a widely used technique in multivariate statistical analysis that employs explanatory methods to elucidate the associations between variables (Yongming et al., 2006). The coefficients were calculated to examine the correlations between the end members of grain size and their morphoscopic parameters. The analyses were performed utilizing the R Studio environment, which is an open-source software (version 4.0.3, www.rstudio.com). Statistical significance was determined at a significance level of $p < 0.05$. Cluster Analysis (CA) is a statistical method used to categorize objects within a system based on their similarities. The main goal of CA is to identify an optimal grouping where objects within each cluster exhibit high similarity, while the clusters themselves are distinct from one another. In the open-source statistical programming language R Studio (version 4.0.3, http://www.rstudio.com), the "compositions" package is used to convert GSD data into the clr-transformed dataset. The PCA and CA were conducted utilizing the “FactoMineR” and “factoextra” packages in R studio.

https://doi.org/10.5194/egusphere-2026-2347
Preprint. Discussion started: 21 May 2026

3.4 Analysis of dynamic drivers of the region

Coastal barriers are characterized by their dynamic nature and composition of unconsolidated sedimentary materials, which exhibit responses to various drivers. These factors encompass short-term influences, such as the effects of low magnitude, high frequency wave and tide processes. In this coastal region, mesotidal conditions and semi-diurnal tidal patterns, the northward movement of a littoral drift system is primarily influenced by waves originating from the south and southeast (Chakrabarti, 2005; Mukherjee et al., 1987; Saha & Sinha, 2023). In contrast, episodic drivers manifest themselves in relation to discrete occurrences, such as fluctuations in wave energy and water levels that transpire during storm events. The significant wave height wind velocity data used in this study were accessed from the Climate Data Store hourly data on single levels from ERA5 dataset (Hersbach et al., 2020).

4. Results

4.1 Variability of grain size distribution of sediment

The grain-size distribution of the first two transects, which are in close proximity to the barrier, exhibits a predominance of sand. The average grain size for these sediments ranges between 2.7 and 4.9 φ (Figure 2). The samples collected from the southwest portion of the transect exhibit a predominant presence of very fine sand particles, whereas the samples obtained from the northeastern sector are primarily composed of coarse-grained sediments. The sediment exhibits relatively poor sorting (Figure 2). In contrast, transects CL-3, CL-4, and CL-5 exhibit the presence of fine-grained sand with moderate to poor sorting (Figure 2). The samples from the northeastern portions of both transects include a significant amount of sand fraction.

https://doi.org/10.5194/egusphere-2026-2347
Preprint. Discussion started: 21 May 2026

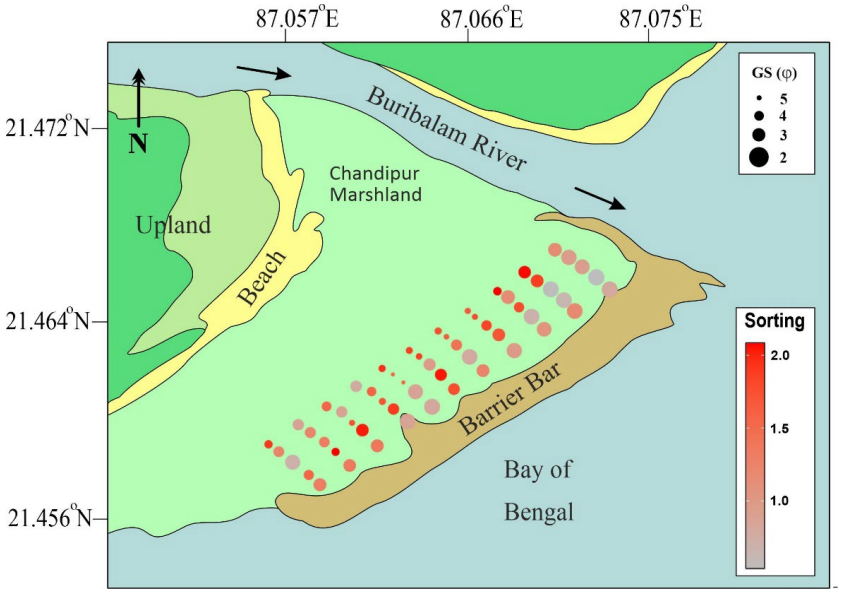

Figure 2: The study area map depicts the average grain size and sorting values of sediments.

4.2 EMMA evaluation of sediments

The diagram depicted in Figure 3 illustrates the end-member (EM) model pertaining to the distribution of grain sizes. The numerical values assigned to the EMs were established within the range of one to ten. The utilization of the coefficient of determination (R^2) and angular deviation served to assess the level of accuracy in fitting the EMs, as well as to ascertain the optimal number in a robust manner. In general, a higher value of R^2 (0.9) and a lower angular degree (5%) correspond to a greater degree of precision in the fitting process. Henceforth, it has been ascertained that four resilient EMs have been discerned within our deposit. The frequency distributions of all four EMs are visually depicted in Figure 3.

https://doi.org/10.5194/egusphere-2026-2347
Preprint. Discussion started: 21 May 2026

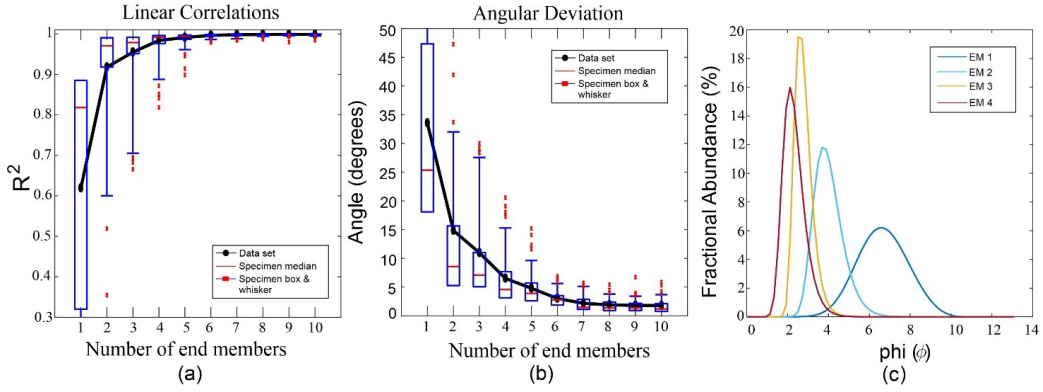

Figure 3: Illustrating the findings obtained from the end-member modeling analysis of the grain size data. The linear correlation (a) and angular deviation (b) between each model size class and the 1–10 end-members was assessed. (C) The grain-size distributions of the modeled end-members from the selected four-end-member model.

The four robust EMs have modal grain sizes of 6.7 φ (EM 1), 4 φ (EM 2), 2.8 φ (EM 3) and 2.4 φ (EM 4), respectively. Figure 4 illustrates the variability of the EMs values observed in the surface sediments. The prevalent distribution of the EM-1 and EM-2 is depicted in Figure 4, away from the bar near the marshland. The EM-3 particle size fraction spreads to a larger section of the CL-3, CL-4, and CL-5 transects of the back-barrier marshland. The sandy EM-4 size fraction predominates in the northeastern and central sectors of the CL-1 and CL-2 transects (Figure 4).

https://doi.org/10.5194/egusphere-2026-2347
Preprint. Discussion started: 21 May 2026

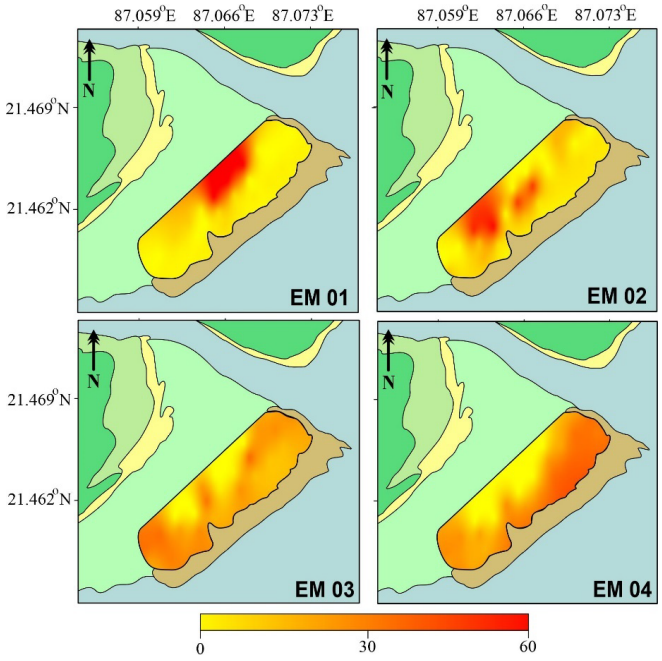

Figure 4: Graph illustrating the spatial representations of the four end-member contributions.

4.3 Variation of the morphoscopic features of the sediment samples

Grain morphoscopic analysis, as outlined in the Cailleux analysis, enables the identification of different sediment types associated with various processes. Both intermediate rounded (EM/EL) and well-rounded (EL) grains with shiny surface were observed in the last three transects (Figure 6). However, the contribution of this set of grains diminishes in the samples closer to the barrier side. The observed prevalence of shiny grains EL and EM/EL in the examined samples from the proximity of marshy region suggests that they have an aqueous origin. The first transect exhibited a predominant presence of intermediate rounded grains, characterized by mostly matte concave parts (EM/RM) (Figure 6). This dominance was also observed in certain sections of the second transect during both sampling periods, as depicted in Figure 5. The grains with a whole matte surface (RM) that exhibit a well-rounded shape are comparatively less abundant when compared to the grains with an angular to subangular shape

https://doi.org/10.5194/egusphere-2026-2347
Preprint. Discussion started: 21 May 2026

271 (EM/RM). These well-rounded grains are primarily found in the southwestern region of the
272 first two transects. This observation implies that the grains have been transported by wind from
273 the adjacent dune and subsequently deposited. The presence of cracked (C) and non-abraded
274 fresh grains (NU) was observed in the northeastern region, and their distribution expanded to
275 the central southeastern back-barrier region (Figure 6). According to previous research, there
276 is a notable resemblance between storm grains and cracked C grains (Martewicz et al., 2022).
277 The prevalence of cracked grains resulting from storm impact exhibited in these sections. The
278 presence of other grains (O) was found to be relatively low, observed only in selected samples
279 from the last two transects in proximity to the marshland.

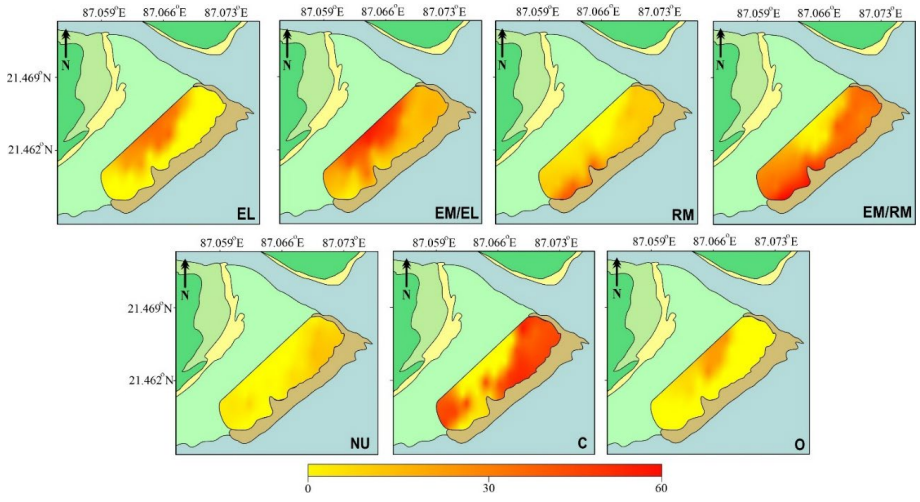

280

281 **Figure 5:** The spatial distribution of frequency distributions of all classes of quartz grains (RM,
282 EM/RM, EL, and EM/EL, NU, C, and O) are presented in these graphs.

https://doi.org/10.5194/egusphere-2026-2347
Preprint. Discussion started: 21 May 2026

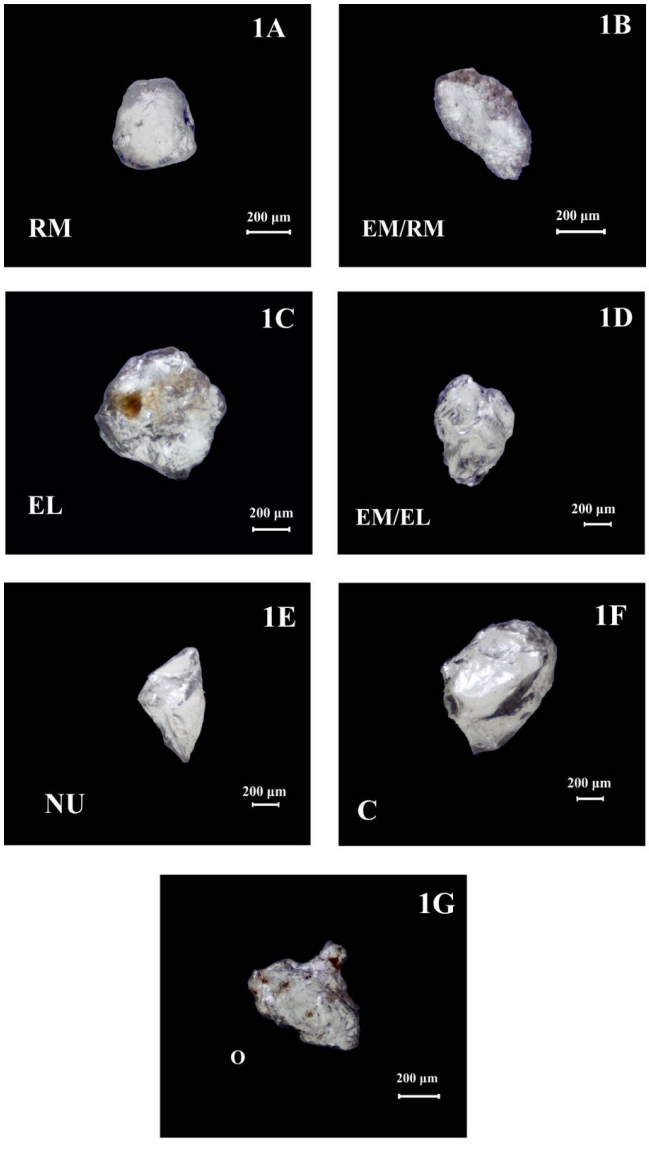

283

284 **Figure 6: The photographs showing quartz grains of different groups according to**
285 **Cailleux analysis under the binocular microscope. The matte surface eolian grain of well-**
286 **rounded (RM) and moderately rounded (EM/RM) nature is observed in 1A, and 1B,**
287 **respectively. The shiny surface containing grains of aqueous origin showing rounded (EL)**
288 **and moderately rounded (EM/EL) shapes is observed in 1C, and 1D, respectively. The**
289 **angular grain with a fresh surface (NU) is shown in 1E. The moderately rounded grain**

https://doi.org/10.5194/egusphere-2026-2347
Preprint. Discussion started: 21 May 2026

with broken surfaces (C) is presented in 1F. 1G shows the irregularly shaped grain containing a weathered surface (O).

4.4 Multivariate statistical analysis

The study employed a principal component analysis (PCA) to examine the interrelationship between the granulometric end members and morphoscopic variables of grains in all samples under investigation. The analysis showed that the first principal component (PC1) explained 39.2% of the total variance, while the second principal component (PC2) explained 33.9% (Figure 7). The first component demonstrated a positive association with the EM1 and EM2 variables, while exhibiting a negative correlation with the EM3 and EM4 variables. The morphoscopic features EL and EM/EL, observed on the aqueous surface, exhibit positive values. Conversely, the morphoscopic feature of the aeolian surface exhibits a significant negative correlation in relation to the first component, as well as a comparable relationship with EM3. In contrast, the EM4 exhibits a positive correlation with the NU and C classifications of grains.

As the outputs of CA suggest, there are three distinctive types (Figure 7). The first cluster grouping, demarcated with 17 samples of blue colour shades, association of the dataset denotes that these samples consist with predominance presence of EM1 and EM2 and subaqueous grains (EL, EM/EL and O). The second sample cluster, represented by the 18 yellow colour samples in Figure 7, exhibited significant contribution of EM3 grain size and aeolian grains (RM, EM/RM). The third type of sample cluster, presented with 20 samples with brown colour, exhibited significant contribution of EM4 grain size and stormy grains (C and NU).

https://doi.org/10.5194/egusphere-2026-2347
Preprint. Discussion started: 21 May 2026

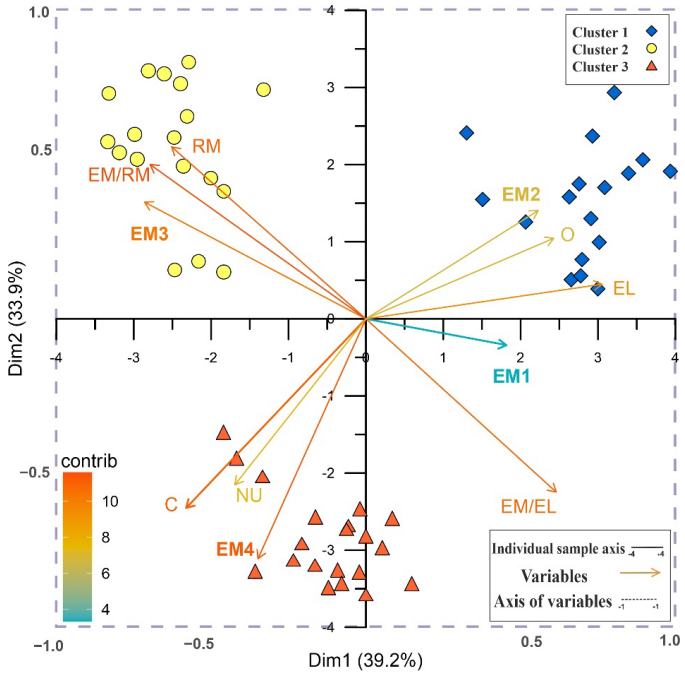

Figure 7: Results from principal component analysis of the granulometric and surface morphoscopic parameters of all of the samples are plotted in this figure.

4.5 Microtextural analysis

Microtextural analyses were conducted by the scanning electron microscope (SEM) images obtained from all samples of third cluster. The grain angularities show a small range in shape on the whisker-box plot, with an average of 3.0 (Figure 8). The grains are mostly subrounded or subangular, with some being angular. The surface features of the samples exhibit a statistical mean of 1.14, indicating that approximately 0 to 15% of the surface portion's grains possess fresh surface features. The coverage of percussion marks across all samples is quite comparable. The mean values of this textural feature vary from 1.7 to 2.4. The adhering particle characteristics of all samples show a distribution mean of 3.9 and a wider distribution range between 3 and 5. The dissolution demonstrates coverage on grains throughout all samples, with a mean of 3.5 to 4.4 and a broader variation spanning from 3 to 5 (Figure 8).

https://doi.org/10.5194/egusphere-2026-2347
Preprint. Discussion started: 21 May 2026

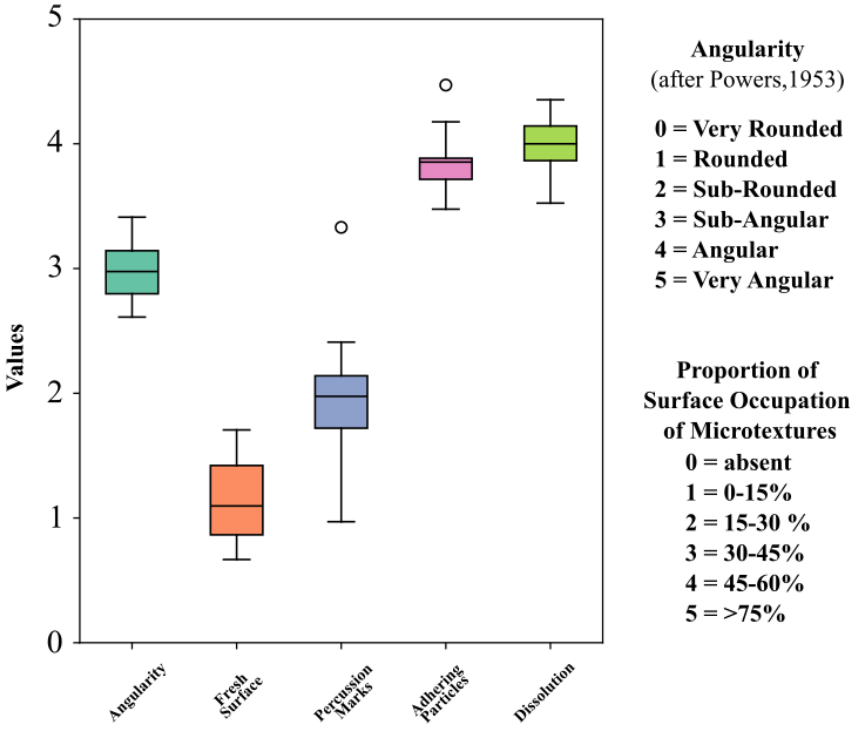

Figure 8: Five important exoscopic microtextural parameters are plotted in this figure. The median value is represented by the central line in the box plot, while the first and third quartiles are indicated by the boundaries of the box.

4.6 Overview of climatic drivers

The region encountered numerous instances of storms during the perilous periods. During 2018, the tropical storm Daye and a Category 3 cyclone Titli had major impacts, along with three deep depressions, Land Depression 02, 03, and 05, as named by the IMD (Supplementary Figure 1). During the occurrence of these events, it was observed that wind velocities reached maximum speeds ranging from 10 to 20 m/s. These storm events were accompanied by a significant increase in wave height compared to non-storm periods, resulting in a surge of high waves that impacted coastal areas in conjunction with the strong winds, which caused the onshore transport of the sediments, dominated by overwash events (Supplementary Figure 2).

https://doi.org/10.5194/egusphere-2026-2347
Preprint. Discussion started: 21 May 2026

5. Discussion

5.1 Detection of the response of the coastal barriers through granulometric end member modelling

The end member EM1, characterized by a modal grain size of 6.7 ϕ, represents the finest size fraction that is deposited from the suspension in the back-barrier marshland. This deposition occurs approximately 200 m inward from the barrier, under calm and quiet conditions. During higher water levels, the presence of a vegetation canopy reduces tidal current velocities, allowing for the deposition of a low-energy, fine-grained fraction (Saha et al., 2024). In contrast, a larger EM2 with a size fraction of 4.0 ϕ is found in the protected areas of the back-barrier marsh. This is primarily influenced by a limited saltation process. The presence of periodic current flow in these regions facilitates the transportation of sediments to the area. In this scenario, sedimentation resulting from suspension continues to be the prevailing depositional process, despite a decrease in the duration of quiescent settling periods. The episodic tidal flow experiences an increase within the regions, which can be attributed to the settling trend and the introduction of a saltation population (Saha et al., 2024). Spatial distribution of clr-transformed EM scores, i.e., clr-EM1 and clr-EM2, suggests a significant contribution of the tidal current deposit in the CL-3, CL- 4 and CL-5 transects, adjacent to the vegetated marshland (Figure 10). The EM3 exhibits a dispersed pattern primarily along the first two transects, with some presence observed along a section of the third transect. According to previous studies, it is most likely that this specific granulometric fraction is transported in the sandy barrier adjacent region through aeolian transportation (Rodriguez et al., 2013; Van Hateren et al., 2020). The transportation of sediment in a landward manner may have occurred through aeolian suspension during favorable weather conditions. Additionally, the strong wind can re-suspend sediment, allowing for the transportation of sandy sediments not only through

https://doi.org/10.5194/egusphere-2026-2347
Preprint. Discussion started: 21 May 2026

saltation but also from suspension and grain fall (Rodriguez et al., 2013). In this scenario, it can be anticipated that as wind speeds surpass a certain threshold, the sediment was transported from the barrier dune. In the back-barrier region, there is significant contribution of clr-transformed EM3 scores in some pockets of the first two transects adjacent to the sandy barrier (Figure 10). The coarser end member EM4 of 2.4 φ represents a sandy overwash deposit that is clearly observed in the back-barrier region through the presence of laminated sand deposits penetrated by the shoots of marsh plants. It is assumed that the storm resultant erosion carries the sand from the intertidal region through the action of surf and swash. This sediment transport is particularly prominent during storm events, when wave and wind motion facilitate the erosion and transportation of the sediment. The clr-transformed EM scores also suggest the northernmost area shows the highest contribution of the washover deposit (EM4). Some samples from the middle portion of these transects also show an increase in the contribution of the overwash sedimentation (Figure 9).

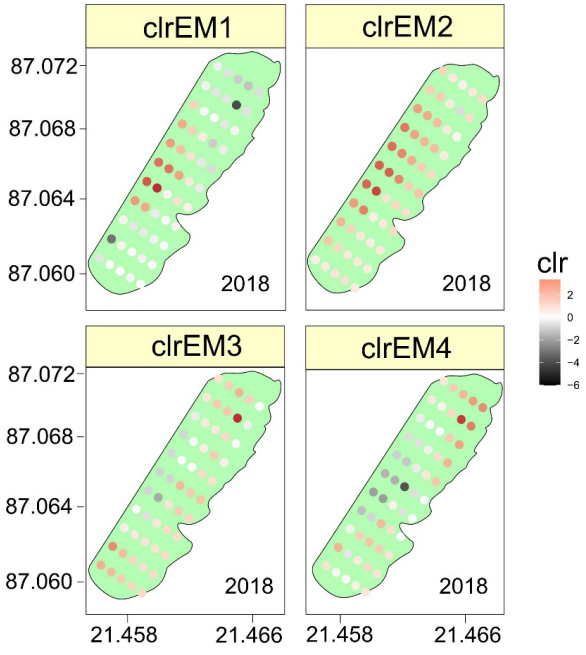

https://doi.org/10.5194/egusphere-2026-2347
Preprint. Discussion started: 21 May 2026

Figure 9: The spatial distribution of the clr-tansformed EM scores is used for understanding the change in the nature of the depositional environment in the back barrier area.

5.2 Characterization of the depositional environment from granulometric and morphoscopic studies

The first cluster, which consists of the blue shades, demonstrates a correlation between the finest fractions EM1, EM2 and the presence of shiny EL and EM/EL grains generated by aqueous processes. The cluster represents a collection of samples that have been deposited under low energy conditions, primarily derived from suspension and saltation deposition (Figure 9). Spatial distribution of the first blue shade suggests significant contribution of the tidal current deposit in the CL-2 and CL-3 transects, adjacent to the vegetated marshland. The finer grades of sediment are deposited in densely vegetated areas where the decreased flow velocities facilitate the settling of grains from suspension, creating a slackwater condition. Moreover, the current flow comprises a significant proportion originating from coarse suspended particles and a limited amount from saltation load. The shift from a state of low energy to a state of high energy occurs when there is an increase in the current flow component, leading to the deposition of most of the sediment from graded suspension.

https://doi.org/10.5194/egusphere-2026-2347
Preprint. Discussion started: 21 May 2026

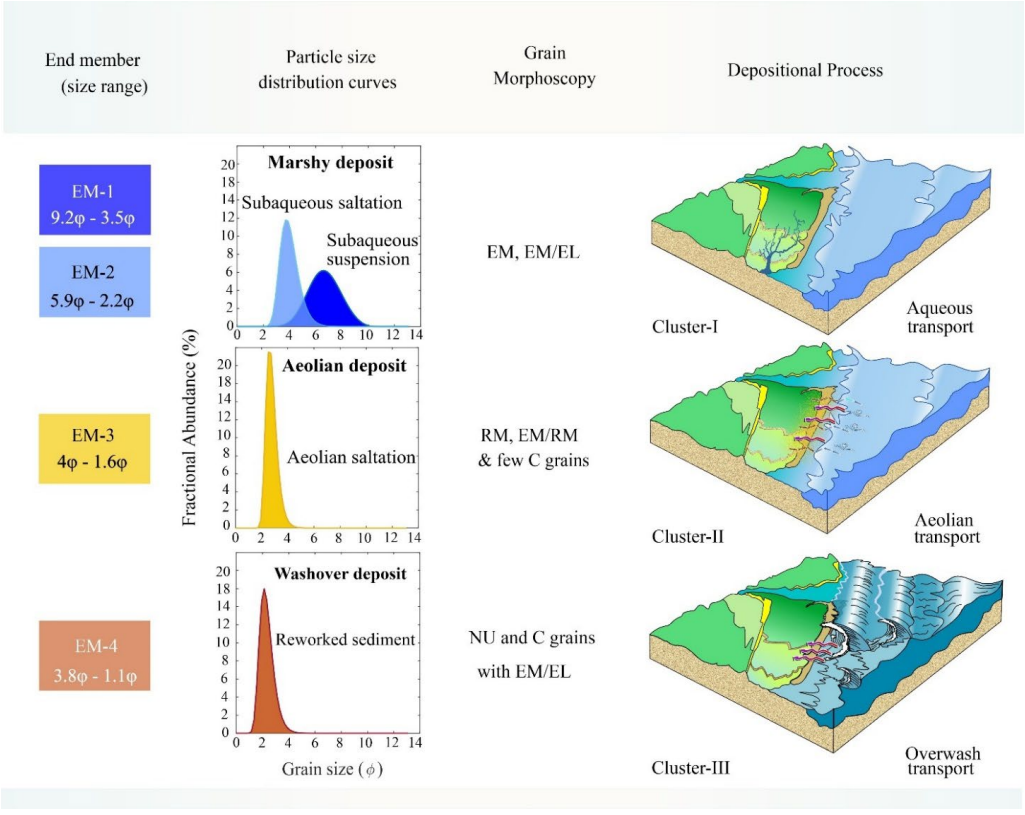

Figure 10: Depositional environments of the coastal region have been classified based on the cluster analysis of the sedimentological proxies. The diagram presents outputs of end member analysis, combined with particle size distribution curves and the predominant morphoscopic characteristics of grains in each depositional environment.

The second cluster, which is delineated by a yellow color, is primarily characterized by a high concentration of fine sand particles in the EM3 size fraction. Additionally, this cluster exhibits a significant abundance of matte RM and EM/RM grains. These samples are dispersed across the eighteen sampling points of the back-barrier region (Figure 10). The transportation of fine to medium sand fractions to the back-barrier marsh via saltation is a significant mechanism, as described in Davidson-Arnott et al. (2019) and Van Hateren et al. (2020). This process involves the launching of sand grains to heights ranging from a few centimeters to 0.5 meters or more,

https://doi.org/10.5194/egusphere-2026-2347
Preprint. Discussion started: 21 May 2026

followed by their downwind movement over distances ranging from a few centimeters to several meters. The transport of aeolian sand to the back-barrier marsh at this location is solely influenced by wind events, specifically during periods of high-speed monsoonal airflow. The scarcity of vegetation in the high-elevation barrier dunes in the adjacent areas is expected to enhance the transport of sand to the back barrier marsh.

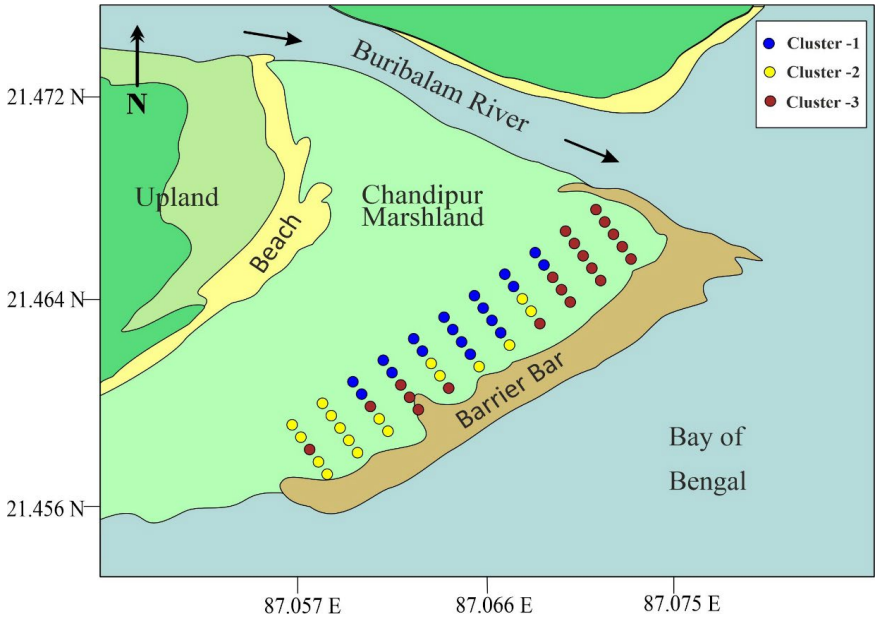

Figure 11: The clustering analysis conducted with the sedimentological proxies of the deposits elucidates the presence of aqueous, aeolian, and washover types of depositional environments.

The third cluster, depicted in brown, is characterized by a predominance of sandy EM4 size fraction and a significant presence of matte C-type cracked and NU grains. These samples extend-across 20 locations, encompassing the north-eastern, central parts of the south-western region (Figure 11). The sediments comprising the analyzed samples have been influenced by storm and cyclone events, resulting in the presence of various quartz grains exhibiting distinct types of shapes and characteristics (Costa et al., 2012). The occurrence of storms affects the sediment flux to the back-barrier marsh at these locations by means of overwash events. During

https://doi.org/10.5194/egusphere-2026-2347
Preprint. Discussion started: 21 May 2026

the process of overwash, a combination of sediment from dunes, beaches, and the shorefaces is deposited as a new washover fan onto an existing marshy deposit located in the specific locations of the study area (Supplementary Figure 2). While cyclone and super cyclone events typically result in significant coastal flooding and overwash, those portions of the back barrier marsh in the Chandipur region was affected by the deposition of washover sands. The sandy washover deposit demonstrates sedimentological attributes that are predominantly unstratified, with an abrupt interface with the marsh sediments. The occurrence of cracked C-type grains identified in the washover deposit could potentially be attributed to the significant collision between grains, which arises from the resuspension and subsequent settling of sand particles due to wave action during overwash events (Figure 11).

5.3 Evaluating the implication of these sedimentological proxies for tempestological investigation

In this sedimentary record, the granulometric and morphoscopic analysis helps to distinguish the washover dominated sedimentary deposits of the back barrier area. Finally, our work highlights the potential of micromorphological analysis alongside these sedimentological proxies for paleotempestological research. Recently, the grain micromorphological analysis is being used in research on storm dynamics. For example, Costa et al. (2012, 2017) Kalińska-Nartiša et al. (2018, 2024) have utilized the mechanical (percussion marks and fresh surfaces) and chemical features (dissolution and adhearing particles), and long-term characteristics (angularity) of sand grains to infer or distinguish storm-derived washover deposits. In accordance with the previous studies, we prioritize the examination of micromorphology to identify storm surge deposits in different environmental settings. The predominant presence of subangular grains is observed (Figure 12A), accompanied by few subrounded grains. The observed samples exhibit a notable prevalence of fresh surfaces, characterized by the presence

https://doi.org/10.5194/egusphere-2026-2347
Preprint. Discussion started: 21 May 2026

of conchoidal fractures of varying sizes within the grains (Figure 12A; 12D; 13D). These grains presented with the greatest number of fresh surfaces, suggesting resurfacing in some portion of the grains due to high-energy clastic collision during stormy events (Figure 12A; 13A). These samples also commonly exhibit v-shaped percussion marks on their surface (Figure 12B; 12F; 13B; 13C), which could have been formed through grain-to-grain collision, a phenomenon commonly observed in high-energy, subaqueous environments like wave action during storm surge events (Ramos-Vázquez and Armstrong-Altrin et al. 2021; Costa et al., 2012; Kalińska-Nartiša et al., 2024). Many grains exhibit a substantial portion of their surface covered with percussion mechanical features. This is contingent upon the concentration of sediment present during the catastrophic transportation process. The higher sediment concentration flows have less intergranular space, resulting in more grain collisions with less kinetic energy and more percussion imprints (Costa et al., 2012;2017). Chemical dissolution features, such as solution pits and oriented etch pits and crevasses are frequently observed in these samples (Figure 12C; 13D). It is plausible that these grains were transported from the nearby coastal area, where they were exposed to alkaline oceanic water for extended durations, leading to the development of these specific chemical dissolution features (Figure 12B; 12C). The presence of adhering particles in these samples indicates the grain collision causes small particles to attach to the surfaces (Figure 12A; 13B). It is likely that these grains have been deposited in the nearshore region through the aqueous transportation/transportation of the Buribulum River and then during catastrophic depositional events, the overwash process resurfaced the preexisting exoscopic features, resulting in the retention of these features on their surfaces. With regard to microtextural signatures, there is a notable increase in the proportion of percussion marks and fresh surfaces observed in storm-produced overwash deposit. This indicates that grains were at least partially resurfaced during transit, even if the distance and period were very short. As reported in an earlier study, the organic and inorganic geochemical proxies have limitations,

https://doi.org/10.5194/egusphere-2026-2347
Preprint. Discussion started: 21 May 2026

and they were ineffective for identifying storm-surge deposits in some coastal environments (Yao et al., 2023). In this context, we can employ microtextural analysis in conjunction with granulometric and grain exoscopic analysis as effective proxies for identifying allochthonous storm deposits of nearshore or offshore origin, as distinct from inshore and local autochthonous deposits within the sediment profile across all littoral environments.

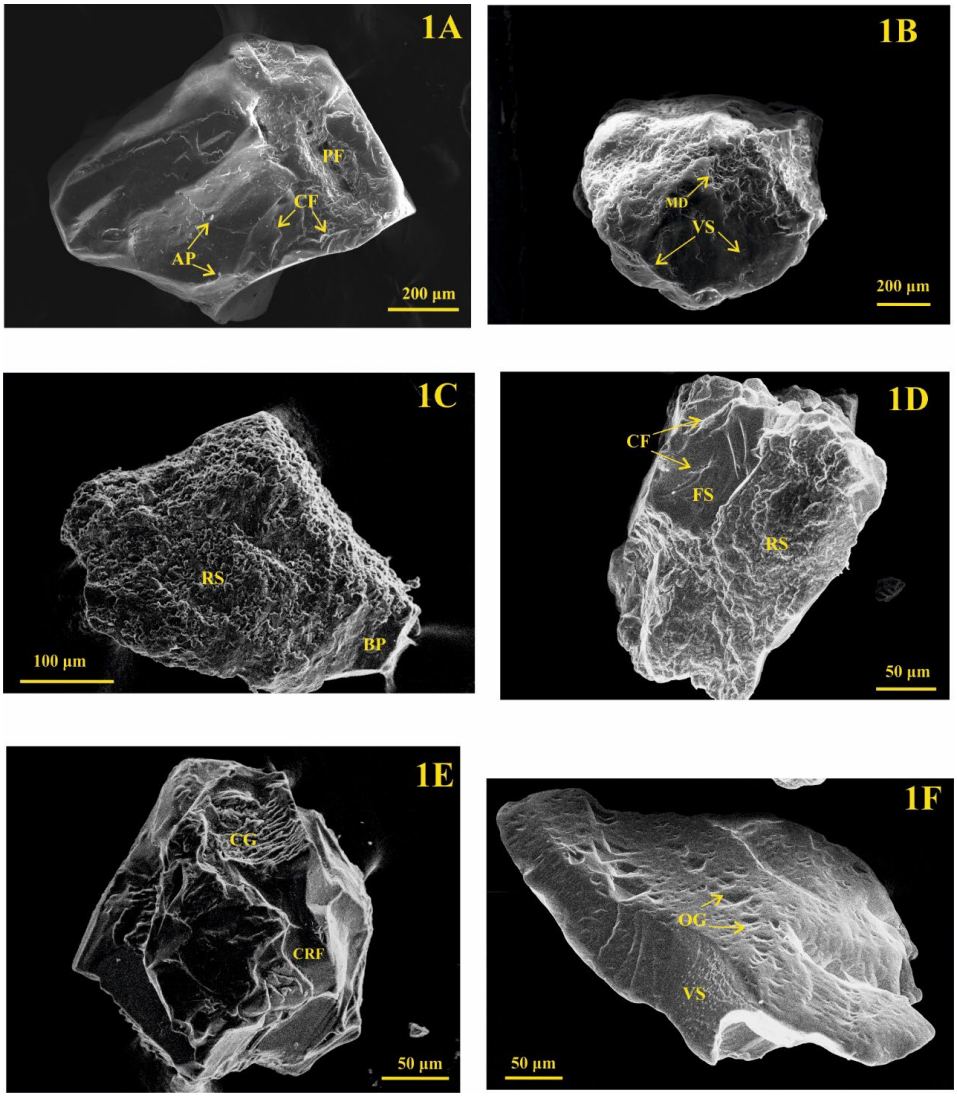

https://doi.org/10.5194/egusphere-2026-2347
Preprint. Discussion started: 21 May 2026

Figure 12: Scanning electron micrographs of the quartz grain surface from stormy clustered samples of the Chandipur, India (A) sub-angular grain with conchoidal fracture (CF). The depressed part on the right side of the grain contains some adhering particles (AP) and precipitation features (PF), probably generated in the nearshore environment. (B) The sand grain contains v-shaped (VS) percussion marks along with un-oriented mechanical depressions (MD). The rounded, protruding grains have been subjected to mechanical action in a subaqueous environment. (C) This subangular grain has a rough surface (RS), probably due to its residence in higher energy subaqueous environments. Although the bottom left corner shows a small broken portion (BP), generated due to collisional impact, (D) The grain shows a mostly rough surface (RS) along with a fracture surface (FS) on the top left side containing various conchoidal fractures (CF). This fracture surface may be generated by intense wave action during storm surges. (E) The sand grains contain a set of curved grooves (CG) in the top portion along with some cracked faces (CRF) on the grains, suggesting collisional breakage of this portion during high energy events. (F) The angular grains of higher relief contain a set of v-shaped (VS) percussion marks on the frontal face. The top surface of this elongated grain contains several oriented grooves (OG), which probably originated due to mechanical collision during strong wave action.

https://doi.org/10.5194/egusphere-2026-2347
Preprint. Discussion started: 21 May 2026

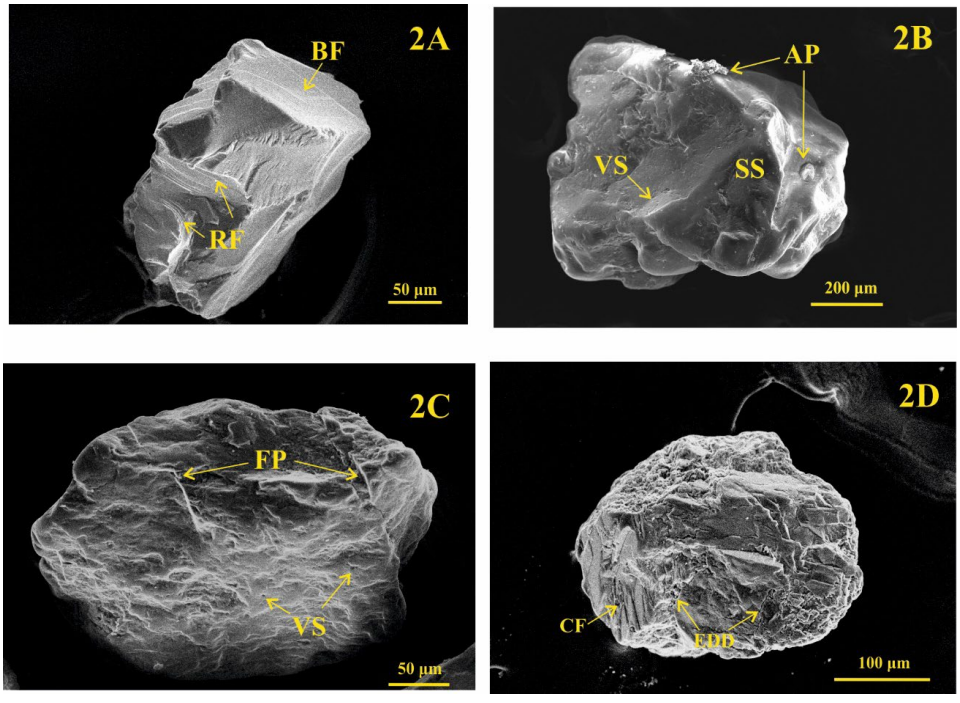

Figure 13: Scanning electron micrographs of the quartz grain from stormy clustered samples of the Chandipur beach, India (A) angular sand grain with high relief showing radial fractures (RF) of different orientations. This type of grain might have been generated by an intergranular attrition. (B) subangular grain showing smooth surfaces (SS) with adhered particles (AP). The mechanical v-shaped (VS) subaqueous depressions are superimposed on the smooth solution precipitation surfaces. Although the shallow nature of the v-shaped depressions appears to have been smoothed by chemical action. Also, some elongated solution pits (SP) are observed in the grains. (C) The subrounded grains show some sub-parallel old fracture planes (FP), which have been modulated to smooth surfaces. Numerous v-shaped marks (VS) are also present on the fracture faces of the grains. (D) The spherical shaped grain contains several conchoidal fractures (CF)

https://doi.org/10.5194/egusphere-2026-2347
Preprint. Discussion started: 21 May 2026

of different sizes and orientations. Additionally, some elongated dissolution depressions (EDD) are observed on the grain surface.

5.4 Implications for shoreline management

The Chandipur coast supports critical mass-nesting grounds of olive ridley sea turtles (Biswas 1981), and the stability of its beaches and adjacent back-barrier wetlands is therefore highly sensitive. Overwash events can rapidly reshape the barrier, alter drainage pathways, and redistribute pollutants, effects known to influence marsh elevation, vegetation structure, and long-term ecosystem resilience (Mariotti et al., 2010; Reed, 1995; Cahoon et al., 2006; Castagno et al., 2021). The sedimentological evidence from this study pinpoints the geomorphic pathways through which these disturbances operate, with overwash-dominated deposits, landward-thinning sheets, and washover fans clearly marking the coastal sectors most frequently reworked by storms. These hazard zones directly overlap with ecologically sensitive habitats, demonstrating how geomorphic instability translates into conservation risk for both turtle rookeries and wetland systems. Such spatially explicit insights are directly applicable to management, enabling authorities to prioritise monitoring in erosion-prone sectors, direct dune-repair or vegetative-stabilization efforts to the most affected areas, and identify where development setbacks or sediment-augmentation interventions are most appropriate. Integrating these sedimentological proxies into a flexible, science-based management framework will enhance the ability to anticipate barrier response under future storm regimes. This approach supports the design of adaptive strategies that sustain habitat integrity, protect critical ecological assets, and balance conservation objectives with the socio-economic needs of the Chandipur coast.

https://doi.org/10.5194/egusphere-2026-2347
Preprint. Discussion started: 21 May 2026

6. Conclusion

Grain size and morphoscopic analysis was used to understand the response of the coastal barrier to tropical storms in the tropical coast of Chandipur, India. We introduce a novel method that can be used to reconstruct sediment transport processes from coastal barrier deposits by using the end-member modelling on grain size distribution. We also evaluated the applicability of grain shape indices following Cailleux analysis to assess the relative contribution of aqueous, aeolian and catastrophically modulated grains to the coastal environment. These spatially distributed various sedimentological proxies are then classified with cluster analysis, which clearly defines the catastrophically deposited surface sediments of the region. Moreover, the scanning electron microscopy also supports the stormy modulations of the quartz grains which show a clear signature of v-shaped percussion marks, dissolution features, various conchoidal fractures, breakage planes and adhering particles. So, this quantitative analysis for understanding the storm and cyclone effects on the coastal barrier region will serve as a modern analogue for understanding the storm effects. Our research can also be used to fathom the inter-seasonal fluctuations of coastal areas, thereby helping to close the knowledge gap and improve the management of coastal modulation initiatives.

https://doi.org/10.5194/egusphere-2026-2347
Preprint. Discussion started: 21 May 2026

Data availability statement:

The data used in the current study will be made available by the corresponding author upon reasonable request.

Acknowledgements

The authors express their gratitude to the scientists of the University Science Instrumentation Centre (USIC), University of North Bengal, for their ongoing support and provision of infrastructural facilities. We would like to express our sincere gratitude to Professor Prasanta Sanyal for his invaluable comments and insightful suggestions.

Financial support

This research did not receive any specific grant from funding agencies in the public, commercial, or not-for-profit sectors.

Declaration of generative AI and AI-assisted technologies in the preparation of this manuscript

During the preparation of this work, the authors used QuillBot (QuillBot, Inc.) to assist with language refinement, grammar correction, and paraphrasing for readability. After using this tool, the authors critically reviewed, edited, and verified all content, and take full responsibility for the content of the publication.

Code availability

End-member modelling (EMMA) was performed using AnalySize v1.1.1 (MATLAB-based). Centered log-ratio (clr) transformation was carried out in R using the *compositions* package.

https://doi.org/10.5194/egusphere-2026-2347
Preprint. Discussion started: 21 May 2026

Author contribution:

KS: conceptualization, methodology, investigation, supervision, formal analysis, writing—original draft. AN: investigation, data curation, visualization, writing—review and editing. KWB: field sampling, data curation, writing—review and editing. JSA-A: validation, interpretation, writing—review and editing."

Competing interests

The authors declare that they have no conflict of interest.

https://doi.org/10.5194/egusphere-2026-2347
Preprint. Discussion started: 21 May 2026

References

565 Aitchison, J.: The statistical analysis of compositional data, *J. R. Stat. Soc. B*, 44, 139–160,
566 1982.
567 Arkema, K. K., Guannel, G., Verutes, G., Wood, S. A., Guerry, A., Ruckelshaus, M., Kareiva,
568 P., Lacayo, M., and Silver, J. M.: Coastal habitats shield people and property from sea-level
569 rise and storms, Nat. Clim. Chang., 3, 913–918, https://doi.org/10.1038/nclimate1944, 2013.
570 Bennington, J. B. and Farmer, E. C.: Recognizing past storm events in sediment cores based
571 on comparison to recent overwash sediments deposited by Superstorm Sandy, in: Learning
572 from the Impacts of Superstorm Sandy, edited by: Bennington, J. B. and Farmer, E. C.,
573 Academic Press, 89–106, https://doi.org/10.1016/B978-0-12-801520-9.00007-9, 2015.
574 Bellanova, P., Bahlburg, H., Nentwig, V., and Spiske, M.: Microtextural analysis of quartz
575 grains of tsunami and non-tsunami deposits – a case study from Tirúa (Chile), Sediment. Geol.,
576 343, 72–84, https://doi.org/10.1016/j.sedgeo.2016.08.001, 2016.
577 Bianchette, T. A., Liu, K.-b., and McCloskey, T. A.: A 4000-year paleoenvironmental
578 reconstruction and extreme event record from Laguna Nuxco, Guerrero, Mexico, Palaeogeogr.
579 Palaeoclimatol. Palaeoecol., 594, 110933, https://doi.org/10.1016/j.palaeo.2022.110933, 2022.
580 Biswas, S.: A report on the olive ridley, Lepidochelys olivacea (Eschscholtz) [Testudines:
581 Cheloniidae] of Bay of Bengal, Rec. Zool. Surv. India, 275–302, 1981.
582 Buccianti, A., Lima, A., Albanese, S., Cannatelli, C., and De Vivo, B.: Exploring topsoil
583 geochemistry from the CoDA (Compositional Data Analysis) perspective: the multi-element
584 data archive of the Campania region (southern Italy), *J. Geochem. Explor.*, 150, 161–172,
585 https://doi.org/10.1016/j.gexplo.2014.12.007, 2015.
586 Bullard, J. E., Ackerley, D., Millett, J., Chandler, J. H., and Montreuil, A.-L.: Post-storm
587 geomorphic recovery and resilience of a prograding coastal dune system, Environ. Res.
588 Commun., 1, 011004, https://doi.org/10.1088/2515-7620/ab0258, 2019.

https://doi.org/10.5194/egusphere-2026-2347
Preprint. Discussion started: 21 May 2026

589 Bushra, N., Trepanier, J. C., and Rohli, R. V.: Joint probability risk modelling of storm surge
590 and cyclone wind along the coast of Bay of Bengal using a statistical copula, Int. J. Climatol.,
591 39, 4206–4217, 2019.
592 Cahoon, D. R.: A review of major storm impacts on coastal wetland elevations, *Estuar. Coasts*,
593 29, 889–898, https://doi.org/10.1007/BF02798648, 2006.
594 Cailleux, A.: Les actions éoliennes périglaciaires en Europe, Mém. Soc. Géol. Fr., 46, 176 pp.,
595 Société géologique de France, 1942.
596 Cailleux, A.: Morphoskopische Analyse der Geschiebe und Sandkörner und ihre Bedeutung
597 für die Paläoklimatologie, Geol. Rundsch., 40, 11–19, 1952.
598 Castagno, K. A., Donnelly, J. P., and Woodruff, J. D.: Grain-size analysis of hurricane-induced
599 event beds in a New England salt marsh, Massachusetts, USA, J. Coast. Res., 37, 326–335,
600 https://doi.org/10.2112/JCOASTRES-D-19-00159.1, 2021.
601 Chakrabarti, A.: Sedimentary structures of tidal flats: a journey from coast to inner estuarine
602 region of eastern India, J. Earth Syst. Sci., 114, 353–368, 2005.
603 Chan, J. C. and Kepert, J. D.: Global perspectives on tropical cyclones: from science to
604 mitigation, World Scientific, Singapore, 2010.
605 Cooper, J. A. G., Green, A. N., and Loureiro, C.: Geological constraints on mesoscale coastal
606 barrier behaviour, Glob. Planet. Change, 168, 15–34, 2018.
607 Cooper, J. A. G. and Pilkey, O. H.: Sea-level rise and shoreline retreat: time to abandon the
608 Bruun Rule, Glob. Planet. Change, 43, 157–171, 2004.
609 Costa, P. J., Andrade, C., Dawson, A., Mahaney, W., Freitas, M., Paris, R., and Taborda, R.:
610 Microtextural characteristics of quartz grains transported and deposited by tsunamis and
611 storms, Sediment. Geol., 275, 55–69, 2012.

https://doi.org/10.5194/egusphere-2026-2347
Preprint. Discussion started: 21 May 2026

612 Costa, P. J. M., Dawson, S., Ramalho, R. S., Engel, M., Dourado, F., Bosnic, I., and Andrade,
613 C.: A review on onshore tsunami deposits along the Atlantic coasts, Earth-Sci. Rev., 212,
614 103441, https://doi.org/10.1016/j.earscirev.2020.103441, 2021.
615 Costa, P. J. M., Gelfenbaum, G., Dawson, S., La Selle, S., Milne, F., Cascalho, J., Ponte Lira,
616 C., Andrade, C., Freitas, M. C., and Jaffe, B.: The application of microtextural and heavy
617 mineral analysis to discriminate between storm and tsunami deposits, Geol. Soc. Spec. Publ.,
618 456, 167–190, https://doi.org/10.1144/SP456.7, 2018.
619 Davidson-Arnott, R., Bauer, B., and Houser, C.: Introduction to Coastal Processes and
620 Geomorphology, 2nd ed., Cambridge University Press, Cambridge,
621 https://doi.org/10.1017/9781108546126, 2019.
622 Dietz, M. E., Liu, K.-b., Bianchette, T. A., Ryu, J., and Yao, Q.: Linking backbarrier lacustrine
623 stratigraphy with spatial dynamics of shoreline retreat in a rapidly subsiding region of the
624 Mississippi River Delta, Geomorphology, 397, 108008, 2022.
625 FitzGerald, D. M., Hein, C. J., Hughes, Z., Kulp, M., Georgiou, I., and Miner, M.: Runaway
626 barrier island transgression concept: global case studies, in: Barrier Dynamics and Response to
627 Changing Climate, edited by: Moore, L. J. and Murray, A. B., Springer, Cham, 3–56,
628 https://doi.org/10.1007/978-3-319-68086-6_1, 2018.
629 Flood, R. P., Orford, J. D., McKinley, J. M., and Roberson, S.: Effective grain size distribution
630 analysis for interpretation of tidal–deltaic facies: West Bengal Sundarbans, *Sediment. Geol.*,
631 318, 58–74, https://doi.org/10.1016/j.sedgeo.2014.12.001, 2015.
632 Haque, Md. M., Ghosh, M. K., and Hoyanagi, K.: Coastal development in southwestern
633 Bangladesh: understanding the interplay between storms and sea level rise, Prog. Phys. Geogr.
634 Earth Environ., 46, 331–356, https://doi.org/10.1177/03091333211046189, 2022.

https://doi.org/10.5194/egusphere-2026-2347
Preprint. Discussion started: 21 May 2026

635 Hawkes, A. D. and Horton, B. P.: Sedimentary record of storm deposits from Hurricane Ike,
636 Galveston and San Luis Islands, Texas, Geomorphology, 171–172, 180–189,
637 https://doi.org/10.1016/j.geomorph.2012.05.017, 2012.
638 Hersbach, H., Bell, B., Berrisford, P., Hirahara, S., Horányi, A., Muñoz-Sabater, J., Nicolas,
639 J., Peubey, C., Radu, R., Schepers, D., Simmons, A., Soci, C., Abdalla, S., Abellan, X.,
640 Balsamo, G., Bechtold, P., Biavati, G., Bidlot, J., Bonavita, M., De Chiara, G., Dahlgren, P.,
641 Dee, D., Diamantakis, M., Dragani, R., Flemming, J., Forbes, R., Fuentes, M., Geer, A.,
642 Haimberger, L., Healy, S., Hogan, R. J., Hólm, E., Janisková, M., Keeley, S., Laloyaux, P.,
643 Lopez, P., Lupu, C., Radnoti, G., de Rosnay, P., Rozum, I., Vamborg, F., Villaume, S., and
644 Thépaut, J.-N.: The ERA5 global reanalysis, Q. J. R. Meteorol. Soc., 146, 1999–2049,
645 https://doi.org/10.1002/qj.3803, 2020.
646 Hong, I., Pilarczyk, J. E., Horton, B. P., Fritz, H. M., Kosciuch, T. J., Wallace, D. J., Dike, C.,
647 Rarai, A., Harrison, M. J., and Jockley, F. R.: Sedimentological characteristics of the 2015
648 tropical cyclone Pam overwash sediments from Vanuatu, South Pacific, Mar. Geol., 396, 205–
649 214, 2018.
650 Hoque, M. A.-A., Sardar, M. L., Sami, M. S., Roy, S., Mukul, S. A., and Pradhan, B.: Mapping
651 tropical cyclone risks in coastal Bangladesh: an integrated geospatial approach, Earth Syst.
652 Environ., 9, 1353–1370, https://doi.org/10.1007/s41748-024-00547-1, 2025.
653 Hossain, H. Z., Armstrong-Altrin, J. S., and Ramos-Vázquez, M. A.: Microtextures on quartz
654 grain surfaces in the Bay of Bengal shoreline sediments, Bangladesh: implications for sediment
655 transport process and depositional environment, *CATENA*, 237, 107770,
656 https://doi.org/10.1016/j.catena.2023.107770, 2024.
657 Johnson, R. A. and Wichern, D. W.: Applied Multivariate Statistical Analysis, 6th ed., Prentice
658 Hall, Upper Saddle River, 2002.

https://doi.org/10.5194/egusphere-2026-2347
Preprint. Discussion started: 21 May 2026

659 Kalińska-Nartiša, E., Stivrins, N., and Grudzinska, I.: Quartz grains reveal sedimentary
660 palaeoenvironment and past storm events: a case study from eastern Baltic, Estuar. Coast. Shelf
661 Sci., 200, 359–370, 2018.
662 Kalińska, E., Weckwerth, P., Lamsters, K., Alexanderson, H., Martewicz, J., and Rosentau, A.:
663 Paleostorm redeposition and post-glacial coastal chronology in the eastern Baltic Sea, Latvia,
664 Geomorphology, 467, 109456, 2024.
665 Ketthong, C., Phantuwongraj, S., Choowong, M., Chutakositkanon, V., and Fujino, S.:
666 Tropical storm event of 4 January 2019 in the Gulf of Thailand: sedimentological comparison
667 to other extreme cyclones and coastal impacts on different shorelines, Earth Syst. Environ., 8,
668 1849–1876, 2024a.
669 Ketthong, C., Phantuwongraj, S., Choowong, M., and Chutakositkanon, V.: Imprints of
670 washover sediments by tropical storm Pabuk 2019 along the coast of the Gulf of Thailand;
671 insight into coastal geomorphological response to storm surge, Mar. Geol., 474, 107321,
672 2024b.
673 Leszczyńska, K., Moskalewicz, D., and Stattegger, K.: Statistical approach to identify storm
674 deposits and cryptic event layers from grain-size data, Mechelinki, Poland, Baltic Sea,
675 *CATENA*, 242, 108130, https://doi.org/10.1016/j.catena.2024.108130, 2024.
676 Machado, G. M. V., Albino, J., Leal, A. P., and Bastos, A. C.: Quartz grain assessment for
677 reconstructing the coastal palaeoenvironment, J. South Am. Earth Sci., 70, 353–367, 2016.
678 Mahaney, W. C.: Atlas of Sand Grain Surface Textures and Applications, Oxford University
679 Press, Oxford/New York, 237 pp., ISBN 0195138120, 2002.
680 Mariotti, G., Fagherazzi, S., Wiberg, P. L., McGlathery, K. J., Carniello, L., and Defina, A.:
681 Influence of storm surges and sea level on shallow tidal basin erosive processes, *J. Geophys.*
682 *Res. Oceans*, 115, C11012, https://doi.org/10.1029/2009JC005892, 2010.

https://doi.org/10.5194/egusphere-2026-2347
Preprint. Discussion started: 21 May 2026

683 Martewicz, J., Kalińska, E., and Weckwerth, P.: What hides in the beach sand? A multiproxy
684 approach and new textural code to recognition of beach evolution on the southern and eastern
685 Baltic Sea coast, Sediment. Geol., 435, 106154, 2022.
686 Masselink, G. and van Heteren, S.: Response of wave-dominated and mixed-energy barriers to
687 storms, Mar. Geol., 352, 321–347, 2014.
688 Mukherjee, K., Das, S., and Chakkrabarti, A.: Common physical sedimentary structures in a
689 beach-related open-sea siliciclastic tropical tidal flat at Chandipur, Orissa, India, and evaluation
690 of the weather conditions through discriminant analysis, Senckenbergiana Marit., 19, 261–293,
691 1987.
692 Mycielska-Dowgiałło, E. and Woronko, B.: Rounding and frosting analysis of quartz sand-
693 grain surfaces and their interpretative significance, Przegl. Geol., 46, 1275–1281, 1998.
694 Mycielska-Dowgiałło, E.: Research methods for textural features of clastic deposits and the
695 significance of interpretational results, in: Research into the Textural Features of Quaternary
696 Sediments and Some Dating Methods, The Family Alliance School of Higher Education Press,
697 Warsaw, 95–180, 2007.
698 Paterson, G. A. and Heslop, D.: New methods for unmixing sediment grain size data, Geochem.
699 Geophys. Geosyst., 16, 4494–4506, 2015.
700 Powers, M. C.: A new roundness scale for sedimentary particles, J. Sediment. Res., 23, 117–
701 119, https://doi.org/10.1306/D4269567-2B26-11D7-8648000102C1865, 1953.
702 Puy, A., Herzog, M., Escriche, P., Marouche, A., Oubana, Y., and Bubenzer, O.: Detection of
703 sand encroachment patterns in desert oases. The case of Erg Chebbi (Morocco), Sci. Total
704 Environ., 642, 241–249, 2018.
705 Rajalakshmi, P. and Achyuthan, H.: Climate change as observed in the Bay of Bengal, J.
706 Climate Change, 7, 69–82, 2021.

https://doi.org/10.5194/egusphere-2026-2347
Preprint. Discussion started: 21 May 2026

Ramos-Vázquez, M. A. and Armstrong-Altrin, J. S.: Provenance of sediments from Barra del Tordo and Tesoro beaches, Tamaulipas State, northwestern Gulf of Mexico, *J. Palaeogeogr.*, 10, 20, https://doi.org/10.1186/s42501-021-00097-0, 2021.

Reed, D. J.: The response of coastal marshes to sea-level rise: survival or submergence?, *Earth Surf. Process. Landf.*, 20, 39–48, https://doi.org/10.1002/esp.3290200105, 1995.

Rodriguez, A. B., Fegley, S. R., Ridge, J. T., VanDusen, B. M., and Anderson, N.: Contribution of aeolian sand to backbarrier marsh sedimentation, Estuar. Coast. Shelf Sci., 117, 248–259, 2013.

Saha, K., Sanyal, P., and Saha, S.: Source assessment of tropical-marshland sediment for evaluating seawater intrusion in Chandipur, India: an integrated granulometric and stable isotope approach, Estuar. Coast. Shelf Sci., 278, 108096, 2022.

Saha, K. and Sinha, S.: Grain size analysis and characterization of sedimentary process in tidal flat of Chandipur region, East Coast of India, Mar. Geodesy, 44, 485–503, 2021.

Saha, K. and Sinha, S.: Distinguishing depositional environments in the beach–dune system of Chandipur, India, based on sediment texture and quartz grain surface features, Earth Surf. Process. Landf., 48, 1251–1266, 2023.

Saha, K., Nandy, A., and Sinha, S.: Unravelling the mesoscale saltmarsh accretion on the tropical barrier estuarine regime: a case study from the Chandipur saltmarsh, India, *Int. J. Sediment Res.*, 39, 458–472, https://doi.org/10.1016/j.ijsrc.2023.09.005, 2024.

Sahoo, B. and Bhaskaran, P. K.: A comprehensive data set for tropical cyclone storm surge-induced inundation for the east coast of India, Int. J. Climatol., 38, 403–419, 2018.

Shanker, K., Pandav, B., and Choudhury, B.: An assessment of the olive ridley turtle (Lepidochelys olivacea) nesting population in Orissa, India, Biol. Conserv., 115, 149–160, 2004.

https://doi.org/10.5194/egusphere-2026-2347
Preprint. Discussion started: 21 May 2026

731 Stewart, H., Bradwell, T., Bullard, J., Davies, S. J., Golledge, N., and McCulloch, R. D.: 8000
732 years of North Atlantic storminess reconstructed from a Scottish peat record: implications for
733 Holocene atmospheric circulation patterns in Western Europe, J. Quat. Sci., 32, 1075–1084,
734 https://doi.org/10.1002/jqs.2983, 2017.
735 van den Boogaart, K. G. and Tolosana-Delgado, R.: "compositions": a unified R package to
736 analyze compositional data, Comput. Geosci., 34, 320–338,
737 https://doi.org/10.1016/j.cageo.2006.11.017 , 2008.
738 Van Hateren, J., Prins, M., and Van Balen, R.: On the genetically meaningful decomposition
739 of grain-size distributions: a comparison of different end-member modelling algorithms,
740 Sediment. Geol., 375, 49–71, 2018.
741 Van Hateren, J. A., Van Buuren, U., Arens, S. M., Van Balen, R. T., and Prins, M. A.:
742 Identifying sediment transport mechanisms from grain size–shape distributions, applied to
743 aeolian sediments, Earth Surf. Dyn., 8, 527–553, 2020.
744 Vos, K., Vandenberghe, N., and Elsen, J.: Surface textural analysis of quartz grains by scanning
745 electron microscopy (SEM): from sample preparation to environmental interpretation, Earth-
746 Sci. Rev., 128, 93–104, 2014.
747 Williams, H.: Contrasting styles of Hurricane Irene washover sedimentation on three east coast
748 barrier islands: Cape Lookout, North Carolina; Assateague Island, Virginia; and Fire Island,
749 New York, Geomorphology, 231, 182–192, 2015.
750 Williams, H. F., Beaubouef, C. E., Liu, K.-b., Culligan, N., and Riedlinger, L.: Testing XRF
751 identification of marine washover sediment beds in a coastal lake in southeastern Texas, USA,
752 Mar. Geol., 443, 106705, 2022.
753 Yang, Y., Piper, D. J., Normandeau, A., Zhou, L., Jia, J., Wang, Y. P., and Gao, S.: A late
754 Holocene shift of typhoon activity recorded by coastal sedimentary archives in eastern China,
755 Sedimentology, 69, 954–969, 2022.

https://doi.org/10.5194/egusphere-2026-2347
Preprint. Discussion started: 21 May 2026

Yao, Q., Liu, K.-b., Wu, Y., Aragón-Moreno, A. A., Rodrigues, E., Cohen, M., de Souza, A. V., Farfán, L. M., and Antinao, J. L.: A multi-proxy record of hurricanes, tsunami, and post-disturbance ecosystem changes from coastal southern Baja California, Sci. Total Environ., 796, 149011, 2021.

Yao, Q., Liu, K.-b., Zhang, Z., Rodrigues, E., Cohen, M., Maiti, K., and Yang, Y.: What are the most effective proxies in identifying storm-surge deposits in paleotempestology? a quantitative evaluation from the sand-limited, peat-dominated environment of the Florida Coastal Everglades, Geochem. Geophys. Geosyst., 24, e2022GC010708, 2023.

Yhasnara, M., Costa, P. J. M., Dourado, F., Martins, M. V. A., Feist, L., Bellanova, P., and Reicherter, K.: Microtextural signatures in quartz grains and foraminifera from tsunami deposits of the Portuguese shelf, Geo-Mar. Lett., 43, 5, https://doi.org/10.1007/s00367-023-00747-0, 2023.

Yongming, H., Peixuan, D., Junji, C., and Posmentier, E. S.: Multivariate analysis of heavy metal contamination in urban dusts of Xi'an, central China, Sci. Total Environ., 355, 176–186, 2006.

Zakir Hossain, H. M., Armstrong-Altrin, J. S., and Ramos-Vázquez, M. A.: Microtextures on quartz grain surfaces in the Bay of Bengal shoreline sediments, Bangladesh: implications for sediment transport process and depositional environment, CATENA, 237, 107770, https://doi.org/10.1016/j.catena.2023.107770, 2024.

Zhang, K., Douglas, B. C., and Leatherman, S. P.: Beach erosion potential for severe nor'easters, J. Coast. Res., 309–321, 2001.

Zhou, L., Gao, S., Jia, J., Zhang, Y., Yang, Y., Mao, L., Fang, X., and Shulmeister, J.: Extracting historic cyclone data from coastal dune deposits in eastern Hainan Island, China, Sediment. Geol., 392, 105524, 2019.

https://doi.org/10.5194/egusphere-2026-2347
Preprint. Discussion started: 21 May 2026

780 Zhou, L., Xu, X., Wang, Y., Jia, J., Yang, Y., Li, G., Tong, C., and Gao, S.: Tracking historical
781 storm records from high-barrier lagoon deposits on the southeastern coast of Hainan Island,
782 China, Acta Oceanol. Sin., 40, 162–175, 2021.
783 Zinnert, J. C., Stallins, J. A., Brantley, S. T., and Young, D. R.: Crossing scales: the complexity
784 of barrier-island processes for predicting future change, BioScience, 67, 39–52, 2017.
785 Zinnert, J. C., Via, S. M., Nettleton, B. P., Tuley, P. A., Moore, L. J., and Stallins, J. A.:
786 Connectivity in coastal systems: barrier island vegetation influences upland migration in a
787 changing climate, Glob. Change Biol., 25, 2419–2430, 2019.